

Article

# Photocatalytic Degradation of Emerging Contaminants with N-Doped TiO<sub>2</sub> Using Simulated Sunlight in Real Water Matrices

Elisa Gaggero, Arianna Giovagnoni, Alessia Zollo, Paola Calza \* and Maria Cristina Paganini 

Department of Chemistry, University of Turin, Via Pietro Giuria 5/7, 10126 Turin, Italy; elisa.gaggero@unito.it (E.G.); arianna.giovagnoni@edu.unito.it (A.G.); alessia.zollo@unito.it (A.Z.); mariacristina.paganini@unito.it (M.C.P.)

\* Correspondence: paola.calza@unito.it

**Abstract:** In the present work, the photodegradation performances of N-doped TiO<sub>2</sub> photocatalysts with enhanced absorption of visible light were exploited for the abatement of some representative contaminants of emerging concern (CECs). Pristine TiO<sub>2</sub> and N-TiO<sub>2</sub> were synthesized using hydrothermal (HT) and sol-gel (SG) routes, they were characterized using XRD and UV-Vis spectroscopy, and their band gaps were determined via analysis in diffuse reflectance. Their photodegradation efficiency was tested on a mixture of recalcitrant organic pollutants, namely, benzotriazole, diclofenac, sulfamethoxazole, and bisphenol A, using a solar simulator lamp with two different cut-off filters ( $\lambda > 340$  nm and  $\lambda > 400$  nm). The evaluation of the photocatalytic performances was initially carried out in spiked ultrapure water and subsequently in aqueous matrices of increasing complexity such as Po River water and water coming from an aquaculture plant. The exclusive utilization of visible light ( $\lambda > 400$  nm) highlighted the advantage of introducing the dopant into the TiO<sub>2</sub> photocatalyst since this modification allows for the material to be responsive to visible light, which is not sufficient in the case of pristine TiO<sub>2</sub> and the higher efficiency of materials obtained via the sol-gel route. Thanks to the doping, improved performance was obtained in both ultrapure water and real water matrices, indicating the potential of the doped material for future applications in the field.

**Keywords:** N-doped TiO<sub>2</sub>; photocatalysis; contaminants of emerging concern



**Citation:** Gaggero, E.; Giovagnoni, A.; Zollo, A.; Calza, P.; Paganini, M.C.

Photocatalytic Degradation of Emerging Contaminants with N-Doped TiO<sub>2</sub> Using Simulated Sunlight in Real Water Matrices. *Inorganics* **2023**, *11*, 439. <https://doi.org/10.3390/inorganics11110439>

Academic Editor: Francis Verpoort

Received: 6 October 2023

Revised: 7 November 2023

Accepted: 15 November 2023

Published: 17 November 2023



**Copyright:** © 2023 by the authors. Licensee MDPI, Basel, Switzerland. This article is an open access article distributed under the terms and conditions of the Creative Commons Attribution (CC BY) license (<https://creativecommons.org/licenses/by/4.0/>).

## 1. Introduction

Freshwater, a limited but renewable resource, is essential for life on Earth. The water cycle replenishes it, but overconsumption can harm ecosystems, and global per capita renewable freshwater resources are declining due to economic development, overexploitation of water resources, pollution, anthropogenic activities, and related climate change. Among the various sources of pollution, the ones with the most significant impact on natural water sources are the agricultural and industrial sources, especially in developing countries [1]. Industrial and domestic wastewater discharges have led to an increase in freshwater pollution and a decrease in clean water resources, particularly in relation to rivers. Rivers can contain microorganisms, heavy metals, and dangerous chemicals, rendering the water unsuitable for direct use and elevating the costs of purification processes [2]. Pollution takes various forms, from aesthetically unpleasant water due to untreated wastewater to organic materials in wastewater causing oxygen depletion and damages to aquatic life [3]. The European Union has identified over a hundred thousand chemical substances as micro-pollutants and generates continuously updated lists of contaminants of emerging concern (CECs) and persistent organic pollutants (POPs). Micro-pollutants encompass items like pharmaceuticals, numerous pesticides, metals, and phthalates [4]. Many commercially available drugs and their byproducts fall under the category of CECs. There has been a global ban on persistent organic pollutants (POPs) since 2004, backed by 179 countries since micro-pollutants are recognized for their non-biodegradability, high toxicity, potential

for bioaccumulation due to their persistent nature, and properties such as genotoxicity, mutagenicity, and oestrogenicity [5,6]. Common micro-pollutants found in groundwater include substances like triclosan, sulfamethoxazole, carbamazepine, and specific pharmaceuticals [7]. Recently, there has been a growing focus of scientific studies on emerging pollutants, leading to the formation of research groups aiming to collect and share detailed information. Their objective is to create management strategies for environmental protection and implement measures to limit pollutants in water environments, alongside technological advancements in water treatment. This interest also arises partly from the lack of regulation for pharmaceutical products and their metabolic byproducts, even if they will likely be subject to future regulations due to their potential impact on both ecosystems and human health. The main concerns lie in the diversity of compounds falling under this category and their proven harmful effects, even at low concentrations. Analytically identifying and removing these substances using conventional methods is challenging since emerging pollutants cover a broad range of compounds, including pharmaceuticals, hormones, pesticides, flame retardants, and fragrances [8]. Addressing their impact may not be simple also because of the difficulty in removing these molecules with conventional techniques. This makes the development of innovative, environmentally friendly, and low-cost systems for their removal essential. In the present work, we aimed at exploiting the photodegradation performances of N-doped TiO<sub>2</sub> photocatalysts with enhanced absorption of visible light for the abatement of some CECs, namely, phenol, bisphenol A, sulfamethoxazole, diclofenac, and benzotriazole, representative of different classes [9–13].

One of the strategies studied and used to degrade emerging pollutants and organic contaminants in water is the employment of visible-light-activated photocatalysts [14–16]. This study focused on four photocatalysts: TiO<sub>2</sub> synthesized through sol–gel and hydrothermal methods, and nitrogen-doped TiO. Among the photocatalysts, TiO<sub>2</sub> is widely studied due to its stability and affordability, though its high band gap limits its efficiency [17,18]. When titanium dioxide absorbs photons compatible with its band gap, it produces hole-electron pairs that allow for the oxidation of water and organic matter and the reduction of oxygen and its reactive species that lead to the formation of radicals that contribute to the further abatement of the contaminants. However, its limited response to visible light restricts its potential; so, to enhance its efficiency, doping with transition metals or non-metals like nitrogen is used [19]. In order to overcome this limitation, nitrogen doping was used. Currently, a substantial body of research results demonstrates that N-doped TiO<sub>2</sub> and N co-doping with transition elements [20–22] exhibit higher photoactivity in visible or solar light compared to the conventional TiO<sub>2</sub>, which serves as the true benchmark for photocatalytic phenomena under the same conditions. However, there is a limited number of experimental studies dedicated to comprehending the underlying reasons for this heightened photoactivity and devising strategies to enhance the photocatalyst's performance (as indicated in references [23–30]). Consequently, it remains uncertain whether this novel material will ultimately be recognized as a significant breakthrough in the realm of photocatalytic applications. To overcome this challenge, it is imperative to devote more attention to both the electronic properties of N-TiO<sub>2</sub> and the mechanisms governing the dynamics of charge carriers during irradiation. Furthermore, such efforts should be aimed at tailoring appropriate modifications of the material to influence its properties. There is now a general consensus on the electronic structure of N-TiO<sub>2</sub> as most of the authors agree on the presence of N 2p intraband gap states some tenths of electronvolts over the valence band (VB) limit. There are currently two distinct categories of photoactive centers that have been identified. The first type arises from the substitution of nitrogen (where nitrogen replaces oxygen in certain lattice positions) and is formed through high-temperature nitridation processes of TiO. The second type, which is more prevalent and occurs in most wet chemistry methods used to prepare the material, involves interstitial nitrogen chemically bonded to a lattice oxygen ion, resulting in the formation of a type of NO group within the bulk of the solid. This species is responsible for the optical absorption in the visible range of N doped titania [31]. Although there is consensus regarding the electronic structure of

N-TiO<sub>2</sub>, there remains a lack of comprehensive understanding concerning how the system behaves in terms of charge dynamics when exposed to visible light. It is of great significance, for instance, to conclusively determine whether visible photons have the capability to induce charge separation, leading to the migration of both electrons and holes at the surface. The presence of electrons and holes at the surface is indeed crucial for initiating the redox processes characteristic of photocatalysis. While the dynamics of charge carriers in photocatalytic systems have primarily been studied using time-resolved spectroscopic techniques in the case of pure TiO<sub>2</sub>, there are relatively few reports available for N-TiO<sub>2</sub> (as mentioned in references [32,33]). In these recent investigations, it has been suggested that the efficiency of charge separation in N-TiO<sub>2</sub> under visible light is, as anticipated, lower than that observed under UV light [34,35].

We assessed the efficiency of the synthesized photocatalysts in degrading persistent organic pollutants using a solar simulator lamp equipped with two distinct cut-off filters ( $\lambda > 340$  nm and  $\lambda > 400$  nm). The evaluation of their photocatalytic effectiveness commenced with pure-water samples spiked with pollutants and progressed to more challenging aqueous environments like Po River water and water from an aquaculture farm.

## 2. Results and Discussion

### 2.1. XRD and UV-VIS Characterization

The synthesized materials were characterized through XRD and Diffuse Reflectance UV Vis analysis.

Figure 1 shows the X-ray diffraction patterns for the photocatalysts obtained using sol-gel and hydrothermal methodologies. As expected, the XRD diffractograms of the nitrogen-doped sample are almost completely overlapping the spectrum of the reference, TiO<sub>2</sub>. The patterns of the two kinds of syntheses present different features. The sol-gel process leads to well crystallized materials with a relatively large size of the crystallites. In the case of pure TiO<sub>2</sub>, some traces of rutile are also present.

In both cases (SG and HT), the diffraction pattern shows a predominance of the anatase phase. This is demonstrated by the presence of peaks at 25.33°, 37.96°, 48.04°, 54.37°, 55.29°, and 62.75° that correspond to the planes of the crystal lattice (101), (004), (200), (105), (211), and (204), respectively [36]. Samples obtained with hydrothermal synthesis also present two peaks that could be assigned to the brookite phase. In general, samples obtained via the hydrothermal method seem to be less crystalline and show smaller crystallites sizes. The presence of Nitrogen is not revealed with this technique, and this is justified by the fact that elements such as N are not visible in X-rays [36]; moreover, it has been demonstrated elsewhere that N species occupy an interstitial position in the lattice of TiO<sub>2</sub> and do not form a periodic phase inside the matrix [25].

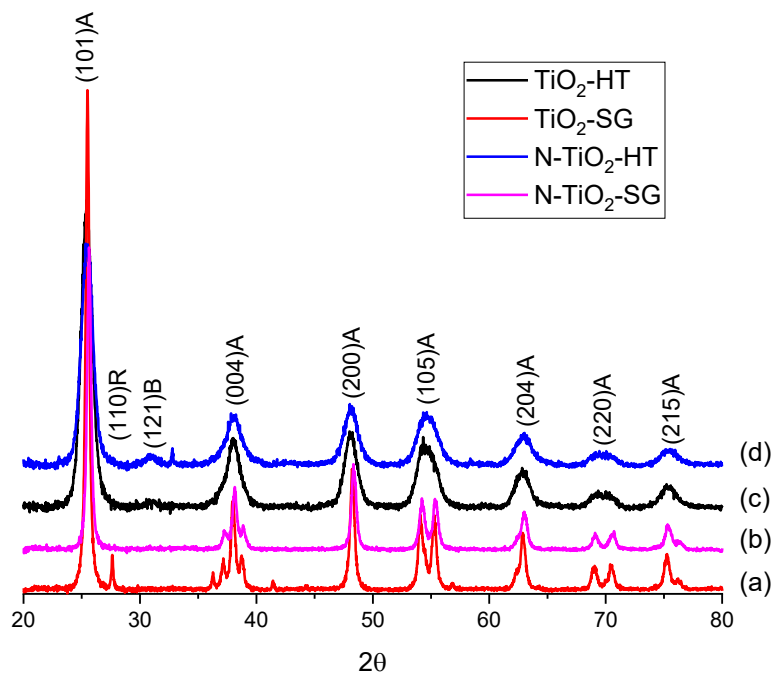
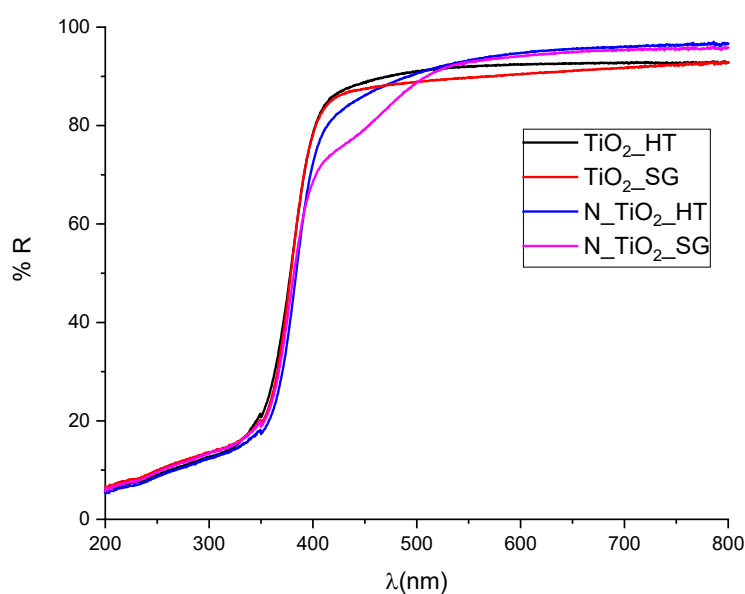
The absorption spectra of the synthesized materials are shown in Figure 2. For the N-doped samples, the absorption due to electronic transitions from a valence band to a conduction band occurring in the UV region and typical of TiO<sub>2</sub> is modified by the onset of a relatively broad absorption band in the visible region whose intensity and width depend on the type of sample. These bands are similar to others reported in the literature [37] for nitrogen-doped TiO<sub>2</sub> and are usually associated with nitrogen insertion in the oxide. It is evident that the N doped sample synthesized via a sol-gel presents the deepest shoulder in the visible region.

From the study on diffuse reflectance, it is possible to determine the band gaps (Table 1) of the materials and highlight any differences due to the presence of the dopant.

The band gap values obtained from processing the Kubelka–Munk function of the spectra using the Tauc plot method highlight that the introduction of nitrogen does not significantly change the band gap value, which remains in the range of 3.34–3.38 eV, around the reference value found in the literature. In fact, the band gap for anatase is 3.2 eV, requiring irradiation with a wavelength  $\lambda < 387$  nm [38].

**Table 1.** Band gap (eV) values determined from absorption spectra for different synthesized materials.

Sample	Band Gap (eV)
TiO <sub>2</sub> -SG	3.38
N-TiO <sub>2</sub> -SG	3.37
TiO <sub>2</sub> -HT	3.37
N-TiO <sub>2</sub> -HT	3.34

**Figure 1.** XRD diffractograms for materials obtained through sol–gel synthesis. (a) TiO<sub>2</sub>-SG, (b) N-TiO<sub>2</sub>-SG and hydrothermal synthesis, (c) TiO<sub>2</sub>-HT, (d) N-TiO<sub>2</sub>-HT. (Together with the prominent anatase phase are also present traces of rutile and brookite phase; residual NH<sub>4</sub>Cl from the synthesis) [39,40].**Figure 2.** DR-UV-Vis spectra for the materials obtained through hydrothermal synthesis TiO<sub>2</sub>-HT and N-TiO<sub>2</sub>-HT, and sol–gel syntheses TiO<sub>2</sub>-SG and N-TiO<sub>2</sub>-SG.

## 2.2. Photocatalytic Degradation of Organic Pollutants

Heterogeneous photocatalysis tests in solution were conducted to determine the photocatalytic activity of the synthesized TiO<sub>2</sub>-based materials. Preliminarily, dark adsorption toward the considered molecules and direct photolysis experiments were carried out with all the materials. Both contributions were found to be negligible over the examined time window. Figure 3 shows the degradation trends of 10 ppm phenol using the synthesized materials under irradiation with a 340 nm cut-off. TiO<sub>2</sub>-based materials doped with nitrogen exhibited excellent photocatalytic performance, leading to complete degradation of phenol within 2 h. It is further inferred that the performance improvement resulting from nitrogen doping is more evident for materials obtained via sol-gel synthesis; this fact could be related to the greater amount of crystalline materials.

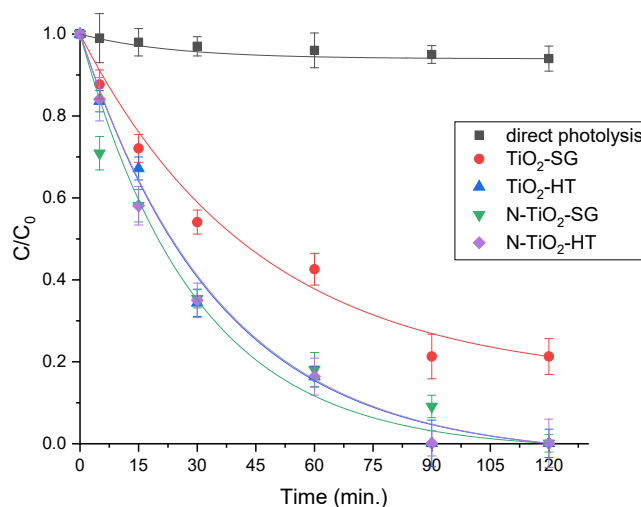


**Figure 3.** Phenol degradation rate using prepared photocatalyst ( $\lambda > 340$  nm).

In order to determine whether nitrogen doping can provide better photocatalytic activity using only visible light, at which the activity of pristine TiO<sub>2</sub> is insufficient because of its high band gap, experiments were repeated by irradiating with a  $\lambda > 400$  nm cut-off. Although the nitrogen-doped materials present the same band gap of the pure titania, the DR UV vis spectra highlighted the presence of an absorption shoulder in the region of the visible light. We know from the literature [31] that this shoulder has been associated with intraband gap states generated from the presence of nitrogen in the lattice of TiO. These states can act as steps for the electrons, so the irradiation with visible light provides enough energy to promote electron migration from the VB to these states and from these states to the CB. Being isolated states, the total efficiency of the process should be expected to be much lower than the classic process from VB to CB.

The kinetic constants of the degradations were calculated by considering the expression of the pseudo-first-order reaction (Equation (1)):

$$\ln \frac{C_t}{C_0} = -kt \quad (1)$$

where  $C_t$  and  $C_0$  are the concentrations at time zero and at any time  $t$  (min), respectively, and  $k$  ( $\text{min}^{-1}$ ) is the rate constant of the equation.

The pseudo first-order kinetic constants and abatement percentage after six hours are reported in Figure 4.

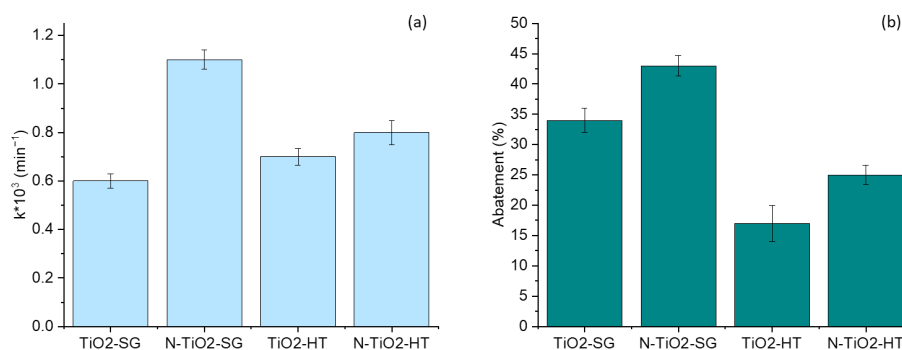


**Figure 4.** Pseudo-first order kinetic constants (a) and abatement percentage (b) after six hours obtained for phenol degradation ( $\lambda > 400 \text{ nm}$ ).

In this case, as expected, lower performances are achieved than using  $\lambda > 340 \text{ nm}$ . In fact, after 90 min, the maximum abatement for N-TiO<sub>2</sub>-HT reached 25% compared to the 100% achieved in the previous case. Interestingly, there is an improvement in the photocatalytic performance of materials obtained via the sol-gel route compared to those obtained via hydrothermal synthesis, presenting an opposite trend in respect to the tests previously carried out. After preliminary tests using phenol as a target molecule, photocatalytic experiments were carried out on a mixture of CECs (benzotriazole, bisphenol A, diclofenac, and sulfamethoxazole) prepared in three matrices of increasing complexity: Milli-Q water, Po river water, and water collected in a koi-carps aquaculture farm. For the actual waters used as matrices, both pH and NPOC values were recorded. The pH was 8.02 and 8.60 for Po River water and water from carp aquaculture, respectively. The NPOC values measured were 1.51 mg/L and 14.2 mg/L for Po River and aquaculture water, respectively.

The activity of all materials was first tested using the  $\lambda > 340 \text{ nm}$  cut-off. Observing the degradation curves reported in Figures S1–S4, it can be pointed out that in the case of hydrothermally obtained materials, abatement around 100% is achieved for all matrices, with no substantial differences between Milli-Q and real waters. Using N-TiO<sub>2</sub>-HT, an abatement greater than 75% is achieved for all contaminants already after the first 60 min and almost-complete abatement in all cases evaluated at the end of the 2-hour experiment. In comparison with the reference, the introduction of nitrogen as a dopant causes a slight increase in the pseudo first-order kinetic constants when real waters are used as matrices.

On the other hand, the performance of the sol-gel-derived materials using a filter at  $\lambda > 340 \text{ nm}$  is inferior to that of hydrothermal-synthesized photocatalysts, particularly when experiments are carried out in aquaculture water; moreover, the introduction of the nitrogen does not appear to positively affect the rate of degradation.

As can be observed in Figure 5, in general, considering pristine materials, a decrease in kinetic constants is registered when moving from Milli-Q water to real water matrices even if the diminution is less pronounced for doped materials. This could be due to the higher content of organic matter and to the presence of naturally occurring inorganic species that can act as scavengers during the oxidation processes, for example, carbonate and bicarbonate ions that can act as scavengers for the hydroxyl radical, reducing the contaminant removal efficiency [41].

With the aim of verifying the performance improvement of the doped material compared to the reference using visible light only, the experiments were repeated using a lamp cut-off that excluded UV-A. In these operating conditions, the advantage of using the doped material is evident from the degradation curves and the abatement values achieved; therefore, using only visible wavelengths reveals the advantage of introducing the dopant inside a photocatalyst such as TiO<sub>2</sub>, which otherwise works mainly in UV-A. Moreover, sol-gel-synthesized photocatalysts exhibit a noticeable increase in degradative capacity compared to hydrothermally obtained materials, confirming what was observed for phenol,

and nitrogen-doped sol-gel photocatalyst shows better performance than the reference and hydrothermal photocatalysts for all CECs monitored and for all matrices studied. The differences between the sol-gel-doped and pure materials are most pronounced for the Milli-Q water matrix and are confirmed by the results obtained in real water matrices. In Milli-Q water, using N-TiO<sub>2</sub>-SG, the complete abatement is achieved for all contaminants within two hours, while for pristine material the degradation rate ranges from 20 to 51% depending on the monitored pollutant. As regards the Po River water matrix, the abatement achieved is between 54% and 68% within two hours for the doped material, whereas it does not exceed 48% for the pristine material. Finally, for the aquaculture water matrix, N-TiO<sub>2</sub>-SG leads to an abatement of at least 70% for all contaminants while it does not exceed 56% for the pristine material. This trend is confirmed by the pseudo first-order kinetic constants' values for the photocatalytic processes, which are always higher than those of the pristine material, in some cases even by an order of magnitude, as shown in Figure 6. Hydrothermal-derived materials also showed improved performance thanks to nitrogen doping, but the degradation efficiency was far lower than that of the sol-gel materials, especially for benzotriazole and bisphenol A. The reason of this difference in the abatement efficiency between the materials obtained with the two synthetic methods can be ascribed to the crystallinity of the prepared samples (much higher in the case of the sol-gel groups than in the case of hydrothermal samples). This explanation can be exhaustive in the case of the pure titania: regarding the abatement activity of N doped samples, it is evident that the SG material is much more active than the HT one. The reason is attributable to the presence of nitrogen in the lattice of titania; in particular, the amount of nitrogen in an interstitial position in the matrix of the SG samples generates enough intraband gap states to allow for electronic migration from VB to these states and from these states to CB, being the energies involved in the range of visible frequencies. In the case of HT doped samples, the amount of nitrogen is not enough to promote a sufficient electronic flow, so it shows a lower photocatalytic activity.

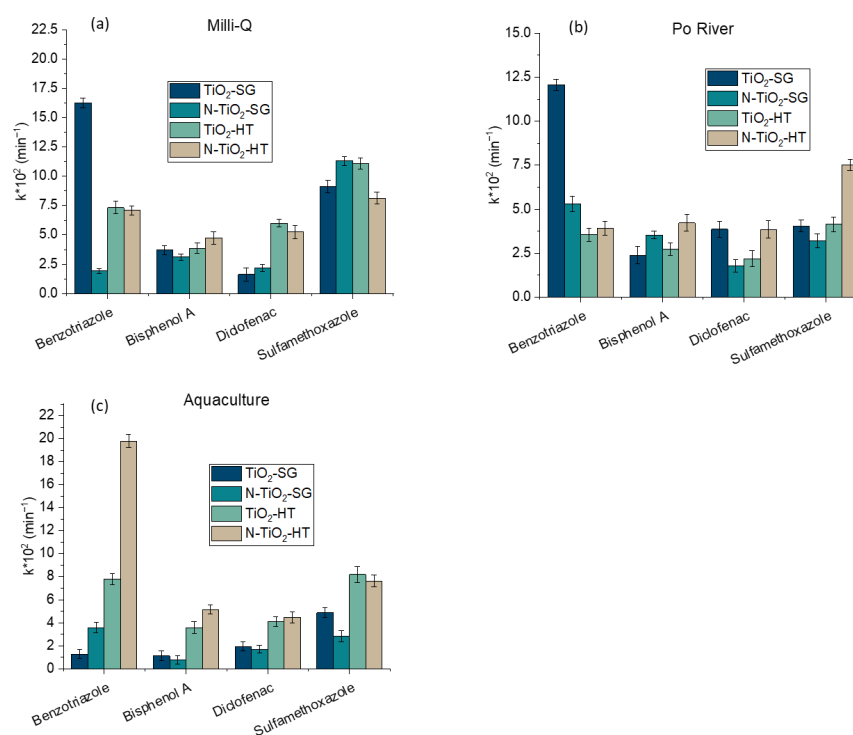


**Figure 5.** Pseudo first-order kinetic constants for the abatement of the mixture of CECs using synthesized photocatalyst, irradiation with  $\lambda > 340$  nm cut-off, and the three matrices: (a) Milli-Q water, (b) Po River water, (c) aquaculture water.

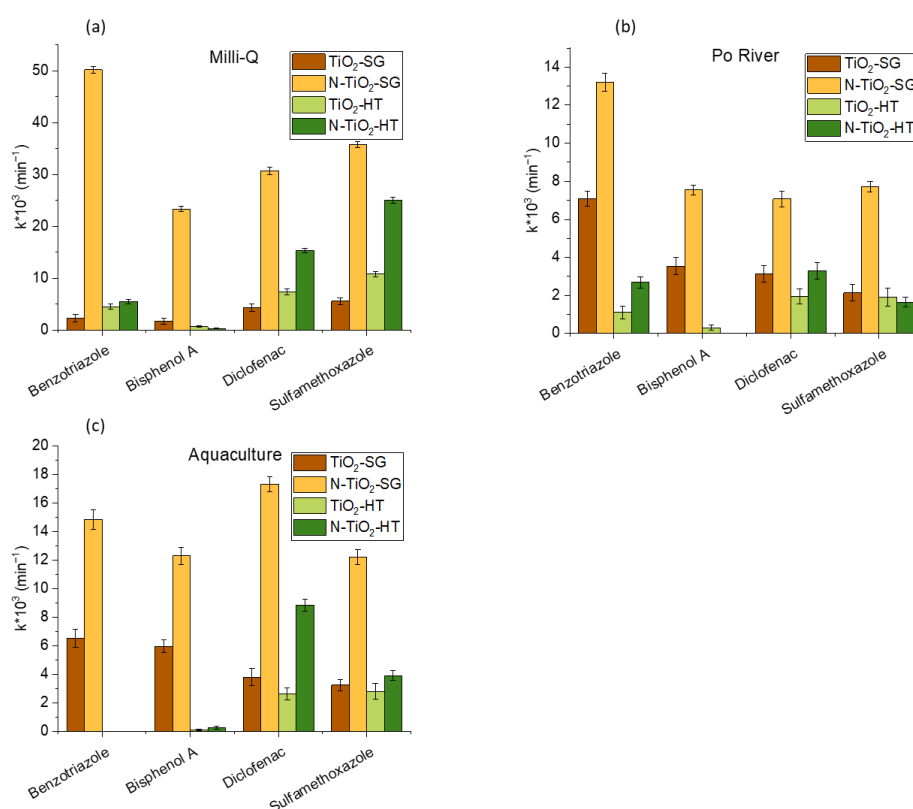


**Figure 6.** Pseudo first-order kinetic constants for the abatement of the mixture of CECs using synthesized photocatalyst, irradiation with  $\lambda > 400$  nm cut-off, and the three matrices: (a) Milli-Q water, (b) Po river water, (c), aquaculture water.

In order to have a broader understanding of the degradation mechanism of the considered pollutants by nitrogen-doped materials, experiments were repeated with irradiation at wavelengths longer than 400 nm using different scavengers. In particular, tert-butyl alcohol, p-benzoquinone, ethylenediaminetetraacetic acid (EDTA), and 2,2,6,6-tetramethylpiperidine (TEMP) were separately added as a scavenger of hydroxyl radicals, superoxide radicals, holes, and singlet oxygen, respectively. Results are reported in Figures S5 and S6 and evidence that depending on the emerging contaminant examined, the reactive species involved in degradation are different, while no substantial dissimilarities are observed between the two materials obtained via the different synthesis routes. In particular, benzotriazole is degraded exclusively by superoxide radicals, while in the degradation of bisphenol A and diclofenac, several reactive species such as superoxide radicals, holes, and singlet oxygen are involved. As for sulfamethoxazole, singlet oxygen, holes, and minimally hydroxyl radicals are involved.

For experiments performed using sol-gel materials on the CECs mixture in Milli-Q water irradiated with a cut-off at 400 nm, the decrease in total organic carbon over time was measured, as shown in Figure 7. Its decrease reflects the degree of mineralization at the end of the photocatalytic process, which is greater for nitrogen-doped materials.

The reason for the remarkable increase in efficiency in the photocatalytic degradation of pollutants for N-doped materials cannot be attributed to a reduction in the band gap because, as demonstrated by the calculated band gap values (Table 1), there is no significant change due to the introduction of the dopant, but rather due to the reduced recombination of photo-generated hole-electron pairs on the material surface; in fact, defects due to oxygen vacancies produced by doping with nitrogen generate intermediate band levels and additional electronic states that can trap electrons and promote absorption into the visible range. It is widely recognized that charge-carrier separation plays a key role in a photocatalytic process, and this, in the present case, results in the increased degradation

efficiency of N-TiO<sub>2</sub>-SG using the visible spectrum due to the generation of intraband gap states produced by the interstitial nitrogen species present both on the surface and in the bulk of the material [42].

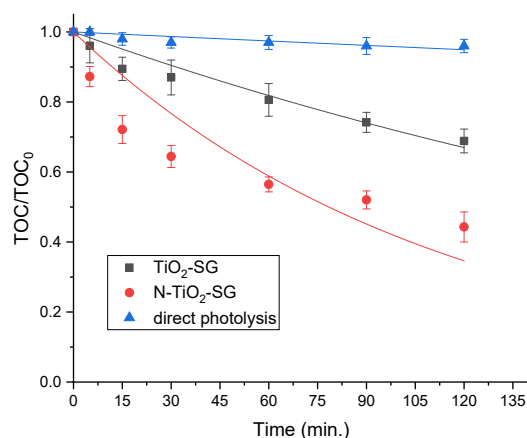


**Figure 7.** TOC abatement of CECs mixture in Milli-Q water using sol-gel materials and irradiation  $\lambda > 400$  nm.

### 3. Materials and Methods

Titanium isopropoxide (97%), 2-propanol ( $\geq 99.5\%$ ), ammonium chloride ( $\geq 99.5\%$ ), potassium permanganate ( $\geq 99\%$ ), fumaric acid ( $\geq 99\%$ ), maleic acid ( $\geq 99\%$ ), phenol ( $\geq 99\%$ ), bisphenol A ( $\geq 99\%$ ), benzotriazole (99%), sulfamethoxazole (analytical standard), and diclofenac sodium salt (pure) were purchased by Sigma Aldrich. All solutions were prepared with ultrapure water Millipore Milli-Q™ (TOC < 2 ppb, conductivity  $\geq 18$  M $\Omega$  cm).

#### 3.1. Synthesis

Four different samples were synthesized: TiO<sub>2</sub> from hydrothermal synthesis (TiO<sub>2</sub>-HT), TiO<sub>2</sub> from sol-gel synthesis (TiO<sub>2</sub>-SG), N-TiO<sub>2</sub> from hydrothermal synthesis (N-TiO<sub>2</sub>-HT), and N-TiO<sub>2</sub> from sol-gel synthesis (N-TiO<sub>2</sub>-SG).

##### 3.1.1. Synthesis of TiO<sub>2</sub> Using Sol-Gel

Precursors were mixed in a 1:1:1 ratio in a 50 mL beaker. Then, 8 mL titanium isopropoxide, 8 mL 2-propanol, and 8 mL deionized water were added [43]. As soon as the water was added under stirring, the gelling process was immediate. After a few minutes of stirring with a magnetic stirrer bar, the beaker was covered and allowed to stand for at least 24 h to ensure cross-linking and thus the correct execution of the sol-gel process. The catalyst obtained was TiO<sub>2</sub> with numerous impurities due to solvent, reagent, and carbon residues. A drying step of at least 4 h in an oven at 70 °C was carried out to remove the most volatile species. Then, the sample was placed in a muffle furnace at 450 °C for 1 h with a ramp of 5 °C/min to remove carbon residues and achieve complete calcination [44].

##### 3.1.2. Synthesis of TiO<sub>2</sub> Using Hydrothermal Method

The hydrothermal method implies shorter times of reaction than the sol-gel method due to the high-pressure and -temperature conditions achieved. The same solution described in the previous paragraph was placed in a Teflon beaker and inserted into an autoclave. The system was placed in the oven for 16 h at 175 °C and then cooled down to ambient temperature. The sample thus collected was washed with deionized water, centrifugated, and dried in the oven at 70 °C for 4 h.

##### 3.1.3. Synthesis of N-TiO<sub>2</sub> Using Sol-Gel Method

Two solutions were prepared: solution A or the mixture of 8 mL of isopropoxide and 8 mL of 2-propanol (1:1 ratio) and solution B that consisted of 0.28 g of ammonium chloride

in 8 mL of water [43]. Once the two solutions were mixed, the gel was allowed to stand for at least 24 h and then dried in the oven at 70 °C for at least 4 h. After that, it was calcined at 450 °C for 1 h in a muffle furnace, exploiting a heating ramp of 5 °C/min.

#### 3.1.4. Synthesis of N-TiO<sub>2</sub> Using Hydrothermal Method

Two solutions were prepared to obtain the desired product: for solution A, 4 mL of isopropoxide and 4 mL of 2-propanol (1:1 ratio) were mixed [43], while for solution B, 0.14 g of NH<sub>4</sub>Cl were added to 4 mL of deionized water. The two solutions were mixed in a Teflon beaker, inserted into an autoclave, and placed in the oven at 175 °C for 16 h. The sample was cooled to room temperature, washed with deionized water, centrifuged, and dried in the oven at 70 °C for 4 h.

### 3.2. Characterization

All synthesized materials were characterized through powder X-ray diffractometry (PXRD) to obtain phase identification and gain information about the crystallinity of the materials. Diffractograms were recorded using the PANalytical PW3040/60 X'Pert Pro MPD instrument, with Bragg–Brentano geometry, equipped with an X-ray generator supplied with a voltage of 45 kV and a current of 40 mA and an X'Celerator scintillation detector. Powder samples were exposed to X Cu K $\alpha$  radiation ( $\lambda = 0.154056$  nm) generated by a ceramic tube with a copper anode, and diffracted beams were collected at  $2\theta$  values between 0 and 180°. The instrument was interfaced to a PC configured with the X'Pert Data Collector and X'Pert HighScore software version 1.0c for recording and interpretation of diffraction data. Diffused Reflectance UV-vis spectroscopy was utilized for the optical characterization of the samples. The optical spectra were captured using a Varian Cary 5000 spectrophotometer (Agilent, CA, USA) and analyzed with the Carywin-UV/scan software version 4.1 (Agilent, CA, USA). A reference sample of PTFE with 100% reflectance was employed. The optical band gap energies were determined using the Tauc plot method applied to the acquired spectra. The energy gap is directly linked to the absorption coefficient near the absorption edge, and its magnitude is contingent upon the nature of the transition (whether direct or indirectly allowed) [45].

### 3.3. Photocatalytic Activity

The photocatalytic activity of the synthesized materials was studied through heterogeneous photocatalysis tests for the degradation of organic pollutants in aqueous solutions. Tests were carried out in Pyrex glass cells of a 5 mL capacity, equipped with a side opening with a screw cap and with a magnetic stirring bar. Substrate solutions and suspensions of each catalyst were prepared in Milli-Q water. The suspensions were put in ultrasonic bath for 30 min before use to make them as homogeneous as possible. The solution containing the organic target and the catalyst suspension was transferred to the cells at a ratio of 1:1. The samples were irradiated for different times (from 0 to 120 min) and then filtered to remove the catalyst and stop the degradation reactions. The filters used were Millipore millex-LCR Hydrophilic PTFE 0.45  $\mu$ m.

An initial evaluation of the photocatalytic activity of the materials was carried out by monitoring the removal of a 10 mg/L phenol solution in Milli-Q water using a concentration of photocatalyst equal to 1 g/L. Photodegradation experiments were conducted inside a Solarbox capable of simulating the spectrum of solar radiation. The Solarbox system, manufactured by CO.FO.ME.GRA., was equipped with a 1500 W Xenon lamp with an irradiance of 19 W/m<sup>2</sup> in the range 295–400 nm. Two different filters were used to select the portion of radiation of interest: one for  $\lambda > 400$  nm, selecting the visible range and excluding UV, and one for  $\lambda > 340$  nm, selecting UV-A and visible.

Furthermore, to gain a deeper understanding of the degradation mechanism of CECs by synthesized photocatalysts, additional experiments at  $\lambda > 400$  nm were conducted, employing different ROS scavengers. Tert-butyl alcohol, p-benzoquinone, ethylenediaminetetraacetic

acid (EDTA), and 2,2,6,6-tetramethylpiperidine (TEMP) were separately added as a scavenger of hydroxyl radicals, superoxide radicals, holes, and singlet oxygen, respectively.

Analyses of organic substrates were performed with an HPLC-UV instrument equipped with a Rheodyne manual injector, two Merck Hitachi L-6200 pumps, a Lichrospher 100 RP C18 column (125 × 4 mm, part-cell diameter 5 μm), and a Merck Hitachi L-4200 single-channel UV-visible detector. The instrument was interfaced to a PC configured with D-7000 HPLC System Manager software version 3.0 for chromatogram monitoring and processing. Then, 10<sup>-2</sup> M orthophosphoric acid buffer (pH 2.8) (A) and acetonitrile (B) were used as eluents for all analyses.

Analyses of phenol photodegradation samples in Milli-Q matrix were performed in isocratic mode with 70:30 A/B at 1 mL/min flow, λ = 220 nm. After the preliminary experiments on phenol, the materials were tested on a mixture of four emerging contaminants, namely, benzotriazole, bisphenol A, diclofenac, and sulfamethoxazole at 4 mg/L each. Milli-Q water, Po River water (sampled on 30 September 2022 in Turin, Valentino Park), and water sampled in an aquaculture plant were used as matrices. The analyses were carried out using the following gradient at 1 mL/min flow: 75:25 A/B for 3 min; 75:25 to 65:35 over 4 min; 65:35 to 40:60 over 8 min; 40:60 for 5 min; 40:60 to 75:25 over 0.5 min; 75:25 for 5 min. The UV detector was set at 220 nm, and the retention times were 2.96, 5.35, 14.08, and 18.20 min for benzotriazole, sulfamethoxazole, bisphenol A, and diclofenac, respectively.

A Shimadzu Total Organic Carbon (TOC) analyzer, model TOC-V CSH, based on catalytic oxidation of carbon on Pt at 680 °C, was used to determine the TOC, so the degree of mineralization of samples containing emerging contaminant mixture after photocatalytic treatment and the Non-purgeable Organic Carbon (NPOC) of real waters were used as matrices.

#### 4. Conclusions

In this study, the synthesis of new TiO<sub>2</sub>-based materials was performed via the hydrothermal and sol-gel routes with the aim of obtaining a doped material efficient in degrading a mixture of emerging contaminants, namely, Benzotriazole, Bisphenol A, Diclofenac, and Sulfamethoxazole, exploiting the use of visible light. The materials obtained were characterized using powder X-ray diffractometry and diffused reflectance UV-vis spectroscopy and tested for the degradation of phenol and mixture of CECs by first irradiating with a lamp equipped with a λ > 340 nm cut-off and then using only the visible spectrum (λ > 400 nm) and matrices of increasing complexity. Based on the results obtained, it can be inferred that when utilizing an irradiation source that encompasses the UV-A component of the solar spectrum, the superiority of the use of doped materials compared to their pristine counterparts is not readily evident, and there is no substantial distinction attributable to the two distinct synthesis approaches. The most evident difference in the materials obtained with the two synthesis approaches is the crystallinity, which is much higher for samples obtained via the sol-gel process. Further analysis will be performed to obtain more information and to better understand the reason for this difference. Conversely, experiments conducted solely with the visible portion of light exhibit a noticeable advantage in the use of nitrogen-doped materials and a heightened efficiency of the photocatalysts produced through the sol-gel method, both in ultrapure and real water. N-TiO<sub>2</sub>-SG emerges as a promising photocatalytic material when exposed to light with a wavelength greater than 400 nm. This is achieved through the introduction of nitrogen that leads to the generation of oxygen vacancies and, more importantly, to the formation of intraband gap states that can play a crucial role in the double-step excitation of the light. These defects give rise to intermediate band levels and extra electronic states, which have the capacity to capture electrons and promote the absorption of visible light, making N-TiO<sub>2</sub>-SG a viable choice for treating contaminated water. In fact, it can be effortlessly synthesized, offering a cost-effective and eco-friendly approach that relies solely on visible light.

**Supplementary Materials:** The following supporting information can be downloaded at: <https://www.mdpi.com/article/10.3390/inorganics11110439/s1>, Figure S1: Degradation curves of benzotriazole using the synthesized photocatalyst in different matrices (a) Milli-Q, (b) Po River, (c) aquaculture water irradiating with lamp equipped with  $\lambda > 340$  nm cut-off. Figure S2. Degradation curves of bisphenol A using the synthesized photocatalyst in different matrices (a) Milli-Q, (b) Po River, (c) aquaculture water irradiating with lamp equipped with  $\lambda > 340$  nm cut-off. Figure S3. Degradation curves of sulfamethoxazole using the synthesized photocatalyst in different matrices (a) Milli-Q, (b) Po River, (c) aquaculture water irradiating with lamp equipped with  $\lambda > 340$  nm cut-off. Figure S4. Degradation curves of diclofenac using the synthesized photocatalyst in different matrices (a) Milli-Q, (b) Po River, (c) aquaculture water irradiating with lamp equipped with  $\lambda > 340$  nm cut-off. Figure S5. The degradation percentage of CECs obtained using N-TiO<sub>2</sub> HT photocatalyst after two hours of irradiation with  $\lambda > 400$  nm in the presence of t-butyl alcohol, p-benzoquinone, EDTA, and TEMP as scavengers of hydroxyl radicals, superoxide radicals, holes, and singlet oxygen, respectively. Figure S6. The degradation percentage of CECs obtained using N-TiO<sub>2</sub> SG photocatalyst after two hours of irradiation with  $\lambda > 400$  nm in the presence of t-butyl alcohol, p-benzoquinone, EDTA, and TEMP as scavengers of hydroxyl radicals, superoxide radicals, holes, and singlet oxygen, respectively.

**Author Contributions:** E.G.: investigation, data curation, writing—original draft, editing; A.G.: investigation; A.Z.: data curation, editing; M.C.P.: conceptualization, writing—review and editing; P.C.: funding acquisition, conceptualization, supervision, writing—review and editing. All authors have read and agreed to the published version of the manuscript.

**Funding:** This research was funded by funding from the European Union's Horizon 2020 Research and Innovation Programme under the MarieSkłodowska-Curie Grant Agreement No101007578 (SusWater).

**Data Availability Statement:** Data, associated metadata, and calculation tools are available from the corresponding author.

**Conflicts of Interest:** The authors declare no conflict of interest.

## References

1. Gleick, P.H. Global Freshwater Resources: Soft-Path Solutions for the 21st Century. *Science* **2003**, *302*, 1524–1528. [[CrossRef](#)]
2. Konar, M.; Evans, T.P.; Levy, M.; Scott, C.A.; Troy, T.J.; Vörösmarty, C.J.; Sivapalan, M. Water resources sustainability in a globalizing world: Who uses the water? *Hydrol. Process.* **2016**, *30*, 3330–3336. [[CrossRef](#)]
3. Chaudhry, F.N.; Malik, M. Factors affecting water pollution: A review. *J. Ecosyst. Ecography* **2017**, *7*, 225–231.
4. Kumar, N.M.; Sudha, M.C.; Damodharam, T.; Varjani, S. Chapter 3-Micro-pollutants in surface water: Impacts on the aquatic environment and treatment technologies. In *Current Developments in Biotechnology and Bioengineering*; Varjani, S., Pandey, A., Tyagi, R.D., Ngo, H.H., Larroche, C., Eds.; Elsevier: Amsterdam, The Netherlands, 2020; pp. 41–62. [[CrossRef](#)]
5. Ashraf, M.A. *Persistent Organic Pollutants (POPs): A Global Issue, a Global Challenge*; Springer: Berlin, Germany, 2017; pp. 4223–4227.
6. Lofrano, G.; Libralato, G.; Meric, S.; Vaiano, V.; Sacco, O.; Venditto, V.; Guida, M.; Carotenuto, M. 1-Occurrence and potential risks of emerging contaminants in water. In *Visible Light Active Structured Photocatalysts for the Removal of Emerging Contaminants*; Sacco, O., Vaiano, V., Eds.; Elsevier: Amsterdam, The Netherlands, 2020; pp. 1–25.
7. Goswami, L.; Kumar, R.V.; Borah, S.N.; Manikandan, N.A.; Pakshirajan, K.; Pugazhenthii, G. Membrane bioreactor and integrated membrane bioreactor systems for micropollutant removal from wastewater: A review. *J. Water Process Eng.* **2018**, *26*, 314–328. [[CrossRef](#)]
8. Salimi, M.; Esrafilii, A.; Gholami, M.; Jafari, A.J.; Kalantary, R.R.; Farzadkia, M.; Kermani, M.; Sobhi, H.R. Contaminants of emerging concern: A review of new approach in AOP technologies. *Environ. Monit. Assess.* **2017**, *189*, 414. [[CrossRef](#)] [[PubMed](#)]
9. Said, K.A.M.; Ismail, A.F.; Karim, Z.A.; Abdullah, M.S.; Hafeez, A. A review of technologies for the phenolic compounds recovery and phenol removal from wastewater. *Process Saf. Environ. Prot.* **2021**, *151*, 257–289. [[CrossRef](#)]
10. Abraham, A.; Chakraborty, P. A review on sources and health impacts of bisphenol A. *Rev. Environ. Health* **2020**, *35*, 201–210. [[CrossRef](#)] [[PubMed](#)]
11. Datta, A.; Alpana, A.; Shrikant, M.; Pratyush, K.; Abhibnav, B.; Ruchita, T. Review on synthetic study of benzotriazole. *GSC Biol. Pharm. Sci.* **2020**, *11*, 215–225. [[CrossRef](#)]
12. Alessandretti, I.; Rigueto, C.V.T.; Nazari, M.T.; Rosseto, M.; Dettmer, A. Removal of diclofenac from wastewater: A comprehensive review of detection, characteristics and tertiary treatment techniques. *J. Environ. Chem. Eng.* **2021**, *9*, 106743. [[CrossRef](#)]
13. Wang, J.; Wang, S. Microbial degradation of sulfamethoxazole in the environment. *Appl. Microbiol. Biotechnol.* **2018**, *102*, 3573–3582. [[CrossRef](#)]
14. Ren, L.; Zhou, W.; Sun, B.; Li, H.; Qiao, P.; Xu, Y.; Wu, J.; Lin, K.; Fu, H. Defects-engineering of magnetic  $\gamma$ -Fe<sub>2</sub>O<sub>3</sub> ultra-thin nanosheets/mesoporous black TiO<sub>2</sub> hollow sphere heterojunctions for efficient charge separation and the solar-driven photocatalytic mechanism of tetracycline degradation. *Appl. Catal. B Environ.* **2019**, *240*, 319–328. [[CrossRef](#)]

15. Rahman, M.U.; Qazi, U.Y.; Hussain, T.; Nadeem, N.; Zahid, M.; Bhatti, H.N.; Shahid, I. Solar driven photocatalytic degradation potential of novel graphitic carbon nitride based nano zero-valent iron doped bismuth ferrite ternary composite. *Opt. Mater.* **2021**, *120*, 111408. [[CrossRef](#)]
16. Hao, Q.; Liu, Y.; Chen, T.; Guo, Q.; Wei, W.; Ni, B. Bi<sub>2</sub>O<sub>3</sub>@ carbon nanocomposites for solar-driven photocatalytic degradation of chlorophenols. *ACS Appl. Nano Mater.* **2019**, *2*, 2308–2316. [[CrossRef](#)]
17. Lee, S.-Y.; Park, S.-J. TiO<sub>2</sub> photocatalyst for water treatment applications. *J. Ind. Eng. Chem.* **2013**, *19*, 1761–1769. [[CrossRef](#)]
18. Gomes, J.; Lincho, J.; Domingues, E.; Quinta-Ferreira, R.M.; Martins, R.C. N–TiO<sub>2</sub> Photocatalysts: A Review of Their Characteristics and Capacity for Emerging Contaminants Removal. *Water* **2019**, *11*, 373. [[CrossRef](#)]
19. Natarajan, T.S.; Mozhiarasi, V.; Tayade, R.J. Nitrogen doped titanium dioxide (N-TiO<sub>2</sub>): Synopsis of synthesis methodologies, doping mechanisms, property evaluation and visible light photocatalytic applications. *Photochem* **2021**, *1*, 371–410. [[CrossRef](#)]
20. Varma, R.; Yadav, M.; Tiwari, K.; Makani, N.; Gupta, S.; Kothari, D.C.; Miotello, A.; Patel, N. Roles of Vanadium and Nitrogen in Photocatalytic Activity of VN-Codoped TiO<sub>2</sub> Photocatalyst. *Photochem. Photobiol.* **2018**, *94*, 955–964. [[CrossRef](#)] [[PubMed](#)]
21. El Koura, Z.; Cazzanelli, M.; Bazzanella, N.; Patel, N.; Fernandes, R.; Arnautakis, G.E.; Gakamsky, A.; Dick, A.; Quaranta, A.; Miotello, A. Synthesis and Characterization of Cu and N Codoped RF-Sputtered TiO<sub>2</sub> Films: Photoluminescence Dynamics of Charge Carriers Relevant for Water Splitting. *J. Phys. Chem. C* **2016**, *120*, 12042–12050. [[CrossRef](#)]
22. Bazzanella, N.; Bajpai, O.P.; Fendrich, M.; Guella, G.; Miotello, A.; Orlandi, M. Ciprofloxacin degradation with a defective TiO<sub>2</sub>-x nanomaterial under sunlight. *MRS Commun.* **2023**, *13*, 1252–1259. [[CrossRef](#)]
23. Nakamura, R.; Tanaka, T.; Nakato, Y. Mechanism for Visible Light Responses in Anodic Photocurrents at N-Doped TiO<sub>2</sub> Film Electrodes. *J. Phys. Chem. B* **2004**, *108*, 10617–10620. [[CrossRef](#)]
24. Li, D.; Haneda, H.; Hishita, S.; Ohashi, N. Visible-light-driven N–F–codoped TiO<sub>2</sub> photocatalysts. 2. Optical characterization, photocatalysis, and potential application to air purification. *Chem. Mater.* **2005**, *17*, 2596–2602. [[CrossRef](#)]
25. Li, D.; Ohashi, N.; Hishita, S.; Kolodiazhnyi, T.; Haneda, H. Origin of visible-light-driven photocatalysis: A comparative study on N/F-doped and N–F-codoped TiO<sub>2</sub> powders by means of experimental characterizations and theoretical calculations. *J. Solid State Chem.* **2005**, *178*, 3293–3302. [[CrossRef](#)]
26. Lin, Z.; Orlov, A.; Lambert, R.M.; Payne, M.C. New Insights into the Origin of Visible Light Photocatalytic Activity of Nitrogen-Doped and Oxygen-Deficient Anatase TiO<sub>2</sub>. *J. Phys. Chem. B* **2005**, *109*, 20948–20952. [[CrossRef](#)] [[PubMed](#)]
27. Nakano, Y.; Morikawa, T.; Ohwaki, T.; Taga, Y. Band-gap narrowing of TiO<sub>2</sub> films induced by N-doping. *Phys. B Condens. Matter* **2006**, *376–377*, 823–826. [[CrossRef](#)]
28. Emeline, A.; Kuzmin, G.; Serpone, N. Wavelength-dependent photostimulated adsorption of molecular O<sub>2</sub> and H<sub>2</sub> on second generation titania photocatalysts: The case of the visible-light-active N-doped TiO<sub>2</sub> system. *Chem. Phys. Lett.* **2008**, *454*, 279–283. [[CrossRef](#)]
29. Emeline, A.V.; Sheremetyeva, N.V.; Khomchenko, N.V.; Ryabchuk, V.K.; Serpone, N. Photoinduced Formation of Defects and Nitrogen Stabilization of Color Centers in N-Doped Titanium Dioxide. *J. Phys. Chem. C* **2007**, *111*, 11456–11462. [[CrossRef](#)]
30. Ohsawa, T.; Lyubinsky, I.; Du, Y.; Henderson, M.A.; Shutthanandan, V.; Chambers, S.A. Crystallographic dependence of visible-light photoactivity in epitaxial TiO<sub>2-x</sub>N<sub>x</sub> anatase and rutile. *Phys. Rev.* **2009**, *79*, 085401. [[CrossRef](#)]
31. Barolo, G.; Livraghi, S.; Chiesa, M.; Paganini, M.C.; Giamello, E. Mechanism of the Photoactivity under Visible Light of N-Doped Titanium Dioxide. Charge Carriers Migration in Irradiated N-TiO<sub>2</sub> Investigated by Electron Paramagnetic Resonance. *J. Phys. Chem. C* **2012**, *116*, 20887–20894. [[CrossRef](#)]
32. Katoh, R.; Furube, A.; Yamanaka, K.-I.; Morikawa, T. Charge Separation and Trapping in N-Doped TiO<sub>2</sub> Photocatalysts: A Time-Resolved Microwave Conductivity Study. *J. Phys. Chem. Lett.* **2010**, *1*, 3261–3265. [[CrossRef](#)]
33. Yamanaka, K.-i.; Morikawa, T. Charge-carrier dynamics in nitrogen-doped TiO<sub>2</sub> powder studied by femtosecond time-resolved diffuse reflectance spectroscopy. *J. Phys. Chem. C* **2012**, *116*, 1286–1292. [[CrossRef](#)]
34. Zhang, Q.; Xiao, Y.; Yang, L.; Wen, Y.; Xiong, Z.; Lei, L.; Wang, L.; Zeng, Q. Branched core-shell a-TiO<sub>2</sub>@ N-TiO<sub>2</sub> nanospheres with gradient-doped N for highly efficient photocatalytic applications. *Chin. Chem. Lett.* **2023**, *34*, 107628. [[CrossRef](#)]
35. Jin, Y.; Zhang, S.; Xu, H.; Ma, C.; Sun, J.; Li, H.; Pei, H. Application of N-TiO<sub>2</sub> for visible-light photocatalytic degradation of *Cylindrospermopsis raciborskii*—More difficult than that for photodegradation of *Microcystis aeruginosa*? *Environ. Pollut.* **2019**, *245*, 642–650. [[CrossRef](#)] [[PubMed](#)]
36. Feng, J.; Bao, W.; Li, L.; Cheng, H.; Huang, W.; Kong, H.; Li, Y. The synergistic effect of nitrogen-doped titanium dioxide/mercaptobenzoic acid/silver nanocomplexes for surface-enhanced Raman scattering. *J. Nanopart. Res.* **2018**, *20*, 82. [[CrossRef](#)]
37. Sato, S. Photocatalytic activity of NO<sub>x</sub>-doped TiO<sub>2</sub> in the visible light region. *Chem. Phys. Lett.* **1986**, *123*, 126–128. [[CrossRef](#)]
38. Asahi, R.; Morikawa, T.; Ohwaki, T.; Aoki, K.; Taga, Y. Visible-Light Photocatalysis in Nitrogen-Doped Titanium Oxides. *Science* **2001**, *293*, 269–271. [[CrossRef](#)] [[PubMed](#)]
39. Swanson, H.E. *Standard X-ray Diffraction Powder Patterns*; US Department of Commerce, National Bureau of Standards: Washington, DC, USA, 1971; Volume 25.
40. Hanawalt, J.D.; Rinn, H.W.; Frevel, L.K. Chemical Analysis by X-ray Diffraction. *Ind. Eng. Chem. Anal. Ed.* **1938**, *10*, 457–512. [[CrossRef](#)]
41. Fernandes, E.; Martins, R.C.; Gomes, J. Photocatalytic ozonation of parabens mixture using 10% N-TiO<sub>2</sub> and the effect of water matrix. *Sci. Total. Environ.* **2020**, *718*, 137321. [[CrossRef](#)]

42. Li, Y.; Peng, Y.-K.; Hu, L.; Zheng, J.; Prabhakaran, D.; Wu, S.; Puchtler, T.J.; Li, M.; Wong, K.-Y.; Taylor, R.A.; et al. Photocatalytic water splitting by N-TiO<sub>2</sub> on MgO (111) with exceptional quantum efficiencies at elevated temperatures. *Nat. Commun.* **2019**, *10*, 1–9. [[CrossRef](#)]
43. Livraghi, S.; Paganini, M.C.; Giamello, E.; Selloni, A.; Di Valentin, C.; Pacchioni, G. Origin of Photoactivity of Nitrogen-Doped Titanium Dioxide under Visible Light. *J. Am. Chem. Soc.* **2006**, *128*, 15666–15671. [[CrossRef](#)]
44. Di Valentin, C.; Pacchioni, G.; Selloni, A.; Livraghi, S.; Giamello, E. Characterization of Paramagnetic Species in N-Doped TiO<sub>2</sub> Powders by EPR Spectroscopy and DFT Calculations. *J. Phys. Chem. B* **2005**, *109*, 11414–11419. [[CrossRef](#)]
45. Tauc, J.; Scott, T.A. The optical properties of solids. *Phys. Today* **1967**, *20*, 105–107. [[CrossRef](#)]

**Disclaimer/Publisher's Note:** The statements, opinions and data contained in all publications are solely those of the individual author(s) and contributor(s) and not of MDPI and/or the editor(s). MDPI and/or the editor(s) disclaim responsibility for any injury to people or property resulting from any ideas, methods, instructions or products referred to in the content.